Analysis of Self-Interference Cancellation under Phase Noise, CFO and IQ Imbalance in GFDM Full-Duplex Transceivers

Analysis of Self-Interference Cancellation Under Phase Noise, CFO, and IQ Imbalance in GFDM Full-Duplex Transceivers

Amirhossein Mohammadian, *Student Member, IEEE*, Chintha Tellambura, *Fellow, IEEE*, and Mikko Valkama, *Senior Member, IEEE*

***Abstract*—This article investigates a full-duplex base station using a generalized frequency division multiplexing (GFDM) transceiver with the radio frequency (RF) impairments including phase noise, carrier frequency offset (CFO) and in-phase (I) and quadrature (Q) imbalance. To fully focus on the RF impairment issue, we study the simple configuration of single uplink user and single downlink user. They both are half-duplex wireless. In the uplink, we study analog and digital self-interference (SI) cancellation and propose a complementary SI suppression method. Desired signal and residual SI powers and signal-to-interference ratio (SIR) are derived in closed form. Similarly, in the downlink, we derive desired signal power, co-channel interference signal power caused by the uplink user and SIR. The RF impairments degrade the efficiency of SI cancellation and affect GFDM more negatively than full-duplex orthogonal frequency division multiplexing (OFDM). Hence, we propose full-duplex GFDM receiver filters for maximizing the SIR for both uplink and downlink transmissions. Finally, the uplink and downlink rates and the uplink-downlink rate region are derived. Significantly, the optimal-filter based GFDM outperforms full-duplex OFDM by 25 dB higher SIR and an uplink rate increase of 500%.**

***Index Terms*—Full-duplex radios, generalized frequency division multiplexing (GFDM), radio frequency (RF) impairments, signal-to-interference ratio (SIR), filter design, rate region.**

I. Introduction

A. Background and Motivation for GFDM and Full-Duplex

WITH the development of full-duplex radios, the simultaneous transmission and reception on the same frequency band can potentially double the network capacity, reduce network delay, and improve network secrecy and the flexibility of spectrum use [1]. However, fifth generation (5G) wireless is a paradigm shift in throughput, latency, and scalability (100 times faster) vis-a-vis the current fourth generation long term evolution (4G-LTE) standard, which uses orthogonal frequency division multiplexing (OFDM). However, OFDM can be overly sensitive to synchronization errors and produce high out-of-band emissions. Moreover, OFDM may not be able meet the physical layer requirements for future services such as massive machine-type communication for the Internet of Things.

Thus, future wireless standards may be supported by generalized frequency division multiplexing (GFDM) [2]. Unlike OFDM, GFDM deliberately allows for non-orthogonal subcarriers, which however creates mutual interference [3]. Indeed, GFDM allows a trade-off between this interference against several benefits. They include digital implementation of filter banks, low peak-to-average power ratio (PAPR) which reduces the hardware cost and power consumption, low out-of-band emissions, high spectral efficiency and low latency [3]. Due to these advantages, GFDM has recently been extensively investigated for cognitive radio networks [4], [5], space-time coding systems [6], filter designs [7], Internet of Things [8], and optical Networks [9]. GFDM also allows for the optimization of pulse shaping filters to enhance desirable performance metrics. Thus, GFDM presents a potential alternative that may achieve the performance targets of 5G wireless and beyond.

In principle, full-duplex base-stations can double spectral efficiency by simultaneously communicating with downlink uplink users over the same band (for cellular full-duplex radios see [10], [11] and references therein). The users can be full-duplex or half-duplex. However, these base stations experience strong self-interference (SI) signals, and the downlink users experience co-channel interference from uplink users. Due to these interference effects, the actual spectral efficiency gains diminish, and it is important to establish the achievable gains. Fortunately, research on full-duplex radios is already appearing. For example, [12] develop estimating and cancelling interference terms to improve the spectral efficiency. In [13], interference alignment is deployed to address the mutual interference. Moreover, the impact of full-duplex radios can be incorporated into other emerging technologies such as massive MIMO (multiple input multiple output). For instance, [14] and [15] consider full-duplex massive MIMO base stations and investigate beam-domain representation of channels and energy harvesting, respectively. Note that this list of papers is not exhaustive, but rapidly evolving.

However, potential spectral efficiency gains of full-duplex radios will erode due to the presence of radio frequency (RF)

Manuscript received August 30, 2019; revised October 29, 2019; accepted October 31, 2019. Date of publication November 15, 2019; date of current version January 15, 2020. The review of this article was coordinated by Dr. Z. Ding. *(Corresponding author: Amirhossein Mohammadian.)*

A. Mohammadian and C. Tellambura are with the Department of Electrical and Computer Engineering, University of Alberta, Edmonton, AB T6G 1H9, Canada (e-mail: am11@ualberta.ca; ct4@ualberta.ca).

M. Valkama is with the Tampere University, Tampere 33720, Finland (e-mail: mikko.valkama@tuni.fi).

Digital Object Identifier 10.1109/TVT.2019.2953623

impairments. Further, comparative evaluations of GFDM and OFDM are needed. These are the goals of this paper.

B. The Problem of Self-Interference

However, full-duplex radios are fundamentally limited by self-interference (SI), which can be as high as 100 dB above the noise floor of the local receiver [16]. Thus, SI must suppressed by passive or active cancellations. However, passive methods include spatial isolation, directional separation, and antenna decoupling [17]. In contrast, active cancellation can be analog or digital [18]. Active analog cancellation injects a cancelling signal to the receive signal in order to suppress SI. This injection can be done at RF or at the analog baseband. In contrast, with active digital cancellation, reconstructed digital samples are subtracted from the quantized received signal. It however requires the estimation of the SI channel and the knowledge of transmitted data.

However, even with these cancellation methods, residual SI remains 15 dB higher than the receiver noise floor [19]. One reason is the RF impairments. Phase noise [17], carrier frequency offset (CFO) [20] and in-phase (I) and quadrature (Q) imbalance [21] are three major RF imperfections which introduce inter-carrier interference and inter-symbol interference. The interference terms affect the performance of the system, e.g., reducing the link capacity. By modeling RF impairments with transmit and receive independent Gaussian distortion noises, [22] studies massive MIMO full-duplex relaying and shows that spectral efficiency is reduced in the presence of the RF impairments. These may be due to aging and low-cost components such as oscillators, which introduce short term phase fluctuations (phase noise). Furthermore, with multicarrier modulations such as GFDM and OFDM, CFO between the incoming signal and the local oscillator results in inter-carrier interference. Moreover, IQ imbalance generates an image signal which is about 25 dB below the desired signal [23] but will be an interference nevertheless. Throughout this paper, unless otherwise stated, GFDM and OFDM refer to GFDM full-duplex radio and OFDM full-duplex radio, respectively.

C. RF Impairments on Full-Duplex OFDM and GFDM

Impact of RF impairments on OFDM full-duplex transceivers has been widely studied. References [17] and [24] clearly show that phase noise impairs SI cancellation, e.g., 30 dB SI increase due to phase noises of two independent oscillators (for up/down conversions). Reference [21] proposes widely-linear digital SI cancellation to compensate for IQ imbalances. Furthermore, the SI and desired channels can be estimated under IQ imbalance [25], and an optimal pilot matrix is proposed. CFO estimation given IQ imbalances is studied in [20]. The collective impact of phase noise and IQ imbalance is investigated in [26]; it is found that with perfect digital domain cancellation, the average SI power increases linearly with 3-dB phase noise bandwidth and IQ image rejection ratio (IRR). Moreover, [23] develops the maximum likelihood estimates of the intended channel, SI channel and RF impairments including the IQ imbalance, power amplifier non-linearity and phase noise.

The rate region of the OFDM full-duplex transceiver is analyzed in [27]–[29]. In [27], rate regions of half-duplex and full-duplex OFDM are compared, and several power allocation algorithms are proposed. Moreover, the achievable sum rates of half-duplex and full-duplex OFDM in the presence of non-ideal conditions are studied in [28]. In [29], phase noise impact on digital cancellation capability of full-duplex OFDM is analyzed in terms of the interference-to-noise ratio, common phase error and the channel estimation error, and the achievable rate region is investigated.

Unlike OFDM, GFDM uses non-orthogonal sub-carriers and a pulse shaping filter covering several time-slots. Therefore, the latter may be more affected by RF impairments than the former. Thus, is it better to use GFDM than OFDM? For **GFDM half-duplex** radios, this question has been somewhat investigated. For example, the collective impact of timing offset, CFO and phase noise are studied in [30], and an optimal filter in presence of CFO is designed in [31]. Joint channel and IQ imbalance estimation is considered in [32], which develops an IQ imbalance compensation scheme. The CFO estimation problem for GFDM system is studied in [33], [34] and CFO cancellation techniques are proposed.

D. Problem Tackled in This Paper

On the other hand, for **GFDM full-duplex** radios, such studies are few and far between. For instance, [35] proposes a digital interference cancellation scheme and derives SI power. But it does not consider analog SI cancellation nor analyze the effects of the RF impairments. Furthermore, to the best of our knowledge, a base-station GFDM full-duplex transceiver has not been investigated by considering analog and digital SI cancellations, phase noise, CFO and IQ imbalance. Moreover, the optimization of its performance by designing optimal transmitter and/or receiver filters against RF impairments, which also determine the rate region of it, has remained elusive. These issues have never been investigated as far as we know.

Some preliminary results on these issues can be found in [36], where we model and analyze the GFDM full-duplex transceiver with RF impairments including phase noise, CFO and IQ imbalance for both analog and digital cancellations. Moreover, a receiver filter to maximize the desired signal-to-interference ratio (SIR) for the uplink is proposed. In this current paper, we greatly extend [36] and model a system with both uplink and downlink transmissions and consider the impact of channel estimation error, as well. Moreover, the differences from [36] include optimal filter design problems for maximizing the SIR in uplink and downlink and the analysis of the uplink-downlink rate region given RF impairments.

E. Contribution of This Article

In this paper, we study the performance of the GFDM full-duplex transceiver with phase noise, CFO and IQ imbalance. The transceiver is part of the base station serving an uplink user and a downlink user at the same time and frequency (Fig. 1). However, the two users are half-duplex nodes. Since our main goal is to provide a comprehensive modeling and analysis of the

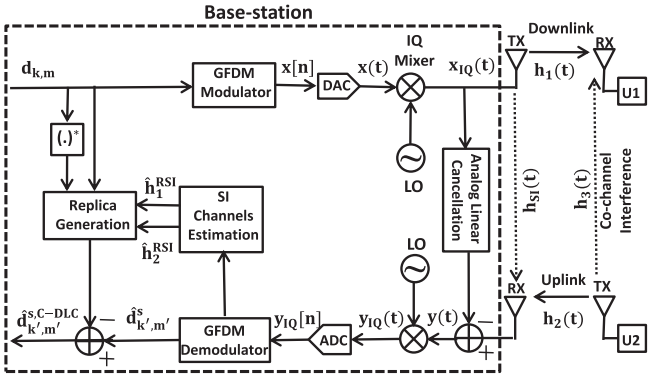

Fig. 1. System model.

transceiver with the RF impairments, we consider two users only. Multi-user scenario are also interesting but are left for future work. The transceiver gets the uplink user signal and leaked own SI signal. Moreover, the received downlink signal contains the base-station intended signal and the uplink co-channel interference signal. These SI, desired and interference channels are modeled as frequency selective, a natural assumption for high data rate systems, where channels become frequency selective. The base-station has two independent local oscillators for up/down conversions and both of them incur IQ imbalances. Moreover, we assume that the uplink user has no RF impairments and downlink user suffers from CFO mismatch only.

More specifically, the following contributions are made:

- We fully model the GFDM full-duplex transceiver with phase noise, CFO and IQ imbalance. Both analog and digital SI cancellation stages are included to develop a complementary digital SI cancellation method.
- In the uplink, we derive residual SI power after analog and digital SI cancellations and desired signal power given the RF impairments. Furthermore, in the downlink, we derive desired signal and co-channel interference signal powers.
- We also derive SIR for both uplink and downlink. We find that GFDM transceiver is more sensitive to the RF impairments than OFDM transceiver. To mitigate this problem, we design optimal receiver filters to maximize the SIR of the GFDM transceiver.
- Rate region is an important concept and refers to the ordered pair of the downlink data rate and uplink data rate. In our problem, these two are mutually dependent because the transmit powers affect both SI and co-channel interference. We derive the rate region by maximizing the uplink rate under the constraint of constant downlink rate. An algorithm for the rate-region computation is also developed.
- All the theoretical derivations are verified with simulation results. Full-duplex GFDM and OFDM transceivers are comparatively evaluated. It is worth mentioning that the collective impact of phase noise, CFO and IQ imbalance has not been investigated previously.

This paper is organized as follows. Section II presents the system model. Section III analyzes the power of uplink and downlink signal components. Section IV formulates the SIRs of uplink and downlink and develops SIR-maximizing receiver filters. Section V derives uplink and downlink rates and solves the rate-region optimization problem. Section VI provides simulation and numerical results to verify the accuracy of the derived results. Finally, Section VII provides the concluding remarks.

II. System Model

As mentioned before, the considered system (Fig. 1) consists of a full-duplex base-station equipped with single separate transmit and receive antennas for serving an uplink user (U_2) and a downlink user (U_1), simultaneously. The system suffers from phase noise, CFO and IQ imbalance. To alleviate SI, we consider analog (RF) linear cancellation and baseband digital linear cancellation. The U_2 transmitter has no phase noise nor IQ imbalance impairments. Moreover, the U_1 receiver has no phase noise and IQ imbalance but has a CFO mismatch. These simplifying assumptions are made in order to isolate and focus on the effects of RF impairments and SI cancellation on the GFDM transceiver. However, U_1 and U_2 may also have various RF impairments. The evaluation of their impact is left for future works. In the following, we analyze the system in detail.

A. Uplink Transmission

The base-station GFDM transceiver generates the transmit signal for M time-slots with K subcarriers. For one symbol time, the discrete GFDM signal may be expressed as

$$x[n] = \sqrt{\alpha} \sum_{k=0}^{K-1} \sum_{m=0}^{M-1} d_{k,m} g_m[n] e^{\frac{j2\pi kn}{K}}, \quad 0 \le n \le MK-1 \tag{1}$$

where α is average transmit power, $\{d_{k,m}\}$ are independent and identically distributed (i.i.d.) complex data symbols with zero mean and unit variance and k is the subcarrier index and m is the time-slot index and $g_m[n] = g[n - mK]_{MK}$ is a circularly shifted version of normalized prototype filter $g[n]$ ($\sum_{n=0}^{MK-1} |g[n]|^2 = 1$). A cyclic prefix is added and digital-to-analog conversion is performed. The analog baseband signal, $x(t)$, is passed through the IQ mixer. I-and Q-branch amplitude and phases mismatches create an undesired signal, which is the mirror image of the original signal. Thus, the IQ mixer output may be written as [21]

$$x_{IQ}(t) = (g_{Tx,d} x(t) + g_{Tx,I} x^*(t)) e^{j\phi_{Tx}(t)} \tag{2}$$

where $(.)^*$ indicates complex conjugate, $g_{Tx,d}$ and $g_{Tx,I}$ are the transmitter IQ mixer responses for the direct and image signals, respectively, and $\phi_{Tx}(t)$ is random phase noise of the local oscillator of the transmitter side. The transmit signal is amplified with a high gain amplifier and sent over the wireless channel. However, part of it appears as SI in the base-station local receiver. Consequently, the received signal in base-station from U_2 could be expressed as

$$\hat{y}(t) = s(t) * h_2(t) + x_{IQ}(t) * h_{SI}(t) + w_2(t) \tag{3}$$

where $*$ denotes the convolution, $s(t)$ is uplink transmit signal from U_2 to base-station, $h_2(t)$ is the uplink multipath channel, $h_{SI}(t)$ is the multipath coupling channel between the local transmitter and the receiver of base-station, and $w_2(t)$ is the additive Gaussian noise with zero mean and variance N_0.

The samples of GFDM signal $s(t)$ may be expressed by (1) with α_s being the average transmit power and with i.i.d. input symbols of $\{d^s_{k,m}\}$. To suppress the SI signal, analog linear cancellation is applied by subtracting the reconstruction signal. Thus, the resulting signal may be expressed as

$$y(t) = s(t) * h_2(t) + x_{IQ}(t) * h_{RSI}(t) + w_2(t) \tag{4}$$

where $h_{RSI}(t) = h_{SI}(t) - h_{ALC}(t)$ is residual SI channel where $h_{ALC}(t)$ is estimate of the the multipath coupling channel. The subscripts RSI and ALC denote residual self-interference and analog linear cancellation. Empirically, 30 dB SI attenuation is possible with analog SI cancellation [24]. Next, $y(t)$ goes through the receiver IQ mixer which, similar to transmitter, has IQ imbalances and produces the image signal. Moreover, we consider CFO between the local oscillators of the transmitter and receiver of base-station. Thus, the signal at the output of the IQ mixer is written as

$$\begin{aligned} y_{IQ}(t) = {} & g_{Rx,d} y(t) e^{-j\phi_{Rx}(t)} e^{j2\pi\Delta_f t} \\ & + g_{Rx,I} y^*(t) e^{j\phi_{Rx}(t)} e^{-j2\pi\Delta_f t} \end{aligned} \tag{5}$$

where $g_{Rx,d}$ and $g_{Rx,I}$ are the receiver IQ mixer responses for the direct and image signals. $\phi_{Rx}(t)$ is random phase noise of the local oscillator of the receiver side and Δ_f indicates the difference between carrier frequency of the receiver and transmitter local oscillators.

IRR quantifies the quality of the IQ mixer which is defined as the ratio between the powers of the IQ mixer response of the image and direct signals $\text{IRR}_{Rx} = \frac{|g_{Rx,I}|^2}{|g_{Rx,d}|^2}$ [21]. According to (2), (3) and (5) and assuming L-tap propagation channels $(h[n] = \sum_{l=0}^{L-1} h_l \delta[n-l])$, the sampled signal could be expressed as

$$\begin{aligned} y_{IQ}[n] = {} & \sum_{l=0}^{L-1} h^I_{RSI}[n,l] x[n-l] + h^Q_{RSI}[n,l] x^*[n-l] \\ & + h^I_2[n,l] s[n-l] + h^Q_2[n,l] s^*[n-l] + w^I_2[n] + w^Q_2[n] \end{aligned} \tag{6}$$

where equivalent channel responses for individual signal components can be written as

$$\begin{aligned} h^I_{RSI}[n,l] = {} & g_{Tx,d} g_{Rx,d} h_{RSI,l} e^{j(\phi_{TX}[n-l] - \phi_{RX}[n])} e^{\frac{j2\pi\epsilon n}{K}} \\ & + g^*_{Tx,I} g_{Rx,I} h^*_{RSI,l} e^{-j(\phi_{TX}[n-l] - \phi_{RX}[n])} e^{\frac{-j2\pi\epsilon n}{K}} \\ h^Q_{RSI}[n,l] = {} & g_{Tx,I} g_{Rx,d} h_{RSI,l} e^{j(\phi_{TX}[n-l] - \phi_{RX}[n])} e^{\frac{j2\pi\epsilon n}{K}} \\ & + g^*_{Tx,d} g_{Rx,I} h^*_{RSI,l} e^{-j(\phi_{TX}[n-l] - \phi_{RX}[n])} e^{\frac{-j2\pi\epsilon n}{K}} \\ h^I_2[n,l] = {} & g_{Rx,d} h_{2,l} e^{-j\phi_{RX}[n]} e^{\frac{j2\pi\epsilon n}{K}} \\ h^Q_2[n,l] = {} & g_{Rx,I} h^*_{2,l} e^{j\phi_{RX}[n]} e^{\frac{-j2\pi\epsilon n}{K}} \\ w^I_2[n] = {} & g_{Rx,d} e^{-j\phi_{RX}[n]} e^{\frac{j2\pi\epsilon n}{K}} w_2[n] \\ w^Q_2[n] = {} & g_{Rx,I} e^{j\phi_{RX}[n]} e^{\frac{-j2\pi\epsilon n}{K}} w^*_2[n] \end{aligned} \tag{7}$$

where ϵ is the normalized CFO by subcarrier spacing. Before deploying digital linear cancellation, the samples are sent to GFDM demodulator where the estimated symbol at $k^{'}$-th subcarrier and $m^{'}$-th time-slot is

$$\widehat{d}^s_{k^{'},m^{'}} = \sum_{n=0}^{MK-1} (y_{IQ}[n]) f_{m^{'}}[n] e^{\frac{-j2\pi k^{'} n}{K}} \tag{8}$$

where $f_{m}[n] = f[n - mK]_{MK}$ is circularly shifted version of receiver filter impulse response $f[n]$. Finally, to further decrease the residual SI signal, we can use the classical digital linear cancellation [21]. This method utilizes the replica of transmitted symbols, $d_{k,'m'}$, and estimation of the equivalent residual SI channel, $\hat{h}^I_{RSI}[n,l]$, and then generates and subtracts digital cancellation symbols from the demodulated symbols. Furthermore, [21] shows that after the classical digital linear cancellation, conjugate SI signal is the dominant source of distortion. Thus, it proposed widely-linear digital SI cancellation method [21] in which SI image components are also attenuated. This method can be done in similar manner as classical digital linear cancellation by this difference that the replica of conjugate of the transmitted symbols, $d^*_{k,'m'}$, and estimation of the equivalent image residual SI channel, $\hat{h}^Q_{RSI}[n,l]$, are utilized to generate digital cancellation symbols. In this paper, we adopt this for full-duplex GFDM and refer to the combination of classical digital linear cancellation and widely-linear digital SI cancellation as complementary digital linear cancellation. The output of complementary digital linear cancellation could be expressed as

$$\begin{aligned} \widehat{d}^{s,C-DLC}_{k^{'},m^{'}} = {} & \left(R^{SI}_{k,'m'} - R^{DLC}_{k,'m'}\right) + \left(R^{SI,im}_{k,'m'} - R^{DLC,i}_{k,'m'}\right) \\ & + R^{s}_{k,'m'} + R^{s,im}_{k,'m'} + w^{eq}_{k,'m'} + w^{eq,im}_{k,'m'} \end{aligned} \tag{9}$$

where $R^{SI}_{k,'m'}$, $R^{SI,im}_{k,'m'}$, $R^{s}_{k,'m'}$, $R^{s,im}_{k,'m'}$, $w^{eq}_{k,'m'}$ and $w^{eq,im}_{k,'m'}$ are corresponding terms for SI signal, desired signal and the equivalent noise after GFDM demodulator that are derived from (1) and (6)–(8). These derivations are omitted due to the space limitation. The superscripts DLC and C-DLC represent digital linear cancellation and complementary digital linear cancellation, respectively. Moreover, $R^{DLC}_{k,'m'}$ and $R^{DLC,i}_{k,'m'}$ are classical digital linear cancellation and widely-linear digital SI cancellation terms, respectively, which are written as

$$\begin{aligned} R^{DLC}_{k,'m'} = {} & \sqrt{\alpha} d_{k,'m'} \sum_{l=0}^{L-1} \sum_{n=0}^{MK-1} \hat{h}^I_{RSI}[n,l] f_{m'}[n] g_{m'} \\ & [n-l] e^{\frac{-j2\pi k^{'} l}{K}} \\ R^{DLC,i}_{k,'m'} = {} & \sqrt{\alpha} d^*_{k,'m'} \sum_{l=0}^{L-1} \sum_{n=0}^{MK-1} \hat{h}^Q_{RSI}[n,l] f_{m'}[n] g^*_{m'} \\ & [n-l] e^{\frac{-j2\pi k^{'} (2n-l)}{K}} \end{aligned} \tag{10}$$

where $\hat{h}^I_{RSI}[n,l]$ and $\hat{h}^Q_{RSI}[n,l]$ indicate equivalent channel estimation of the linear SI signal and the conjugate SI signal, respectively. Note that output of the classical digital linear cancellation is derived by, $\widehat{d}^{s,DLC}_{k^{'},m^{'}} = \widehat{d}^{s,C-DLC}_{k^{'},m^{'}} + R^{DLC,i}_{k,'m'}$. Clearly, the estimated symbol in (9) contains inter carrier interference

and inter symbol interference terms from SI signal and uplink transmitted signal, which are caused by the RF impairments and non-orthogonality of GFDM.

B. Downlink Transmission

The signal received by U_1 in downlink may be written as

$$r(t) = x_{IQ}(t) * h_1(t) + s(t) * h_3(t) + w_1(t) \tag{11}$$

where $h_1(t)$ is downlink multipath channel, $h_3(t)$ is the channel between downlink and uplink users, and $w_1(t)$ is the additive Gaussian noise with zero mean and variance N_0. We assume that the normalized CFO by subcarrier spacing between the oscillators of base-station and U_1 transmitters is equal to ϵ. With the L-tap channels and removal of the cyclic prefix, the discrete samples of the received signal become

$$\begin{aligned} r_{CFO}[n] = &\sum_{l=0}^{L-1} h_1^I[n,l]x[n-l] + h_1^Q[n,l]x^*[n-l] \\ &+ h_{3,l}s[n-l] + w_1[n] \end{aligned} \tag{12}$$

where the equivalent channel responses are given by

$$\begin{aligned} h_1^I[n,l] &= g_{Tx,d}h_{1,l}e^{j\phi_{TX}[n-l]}e^{\frac{j2\pi\epsilon n}{K}} \\ h_1^Q[n,l] &= g_{Tx,I}h_{1,l}e^{j\phi_{TX}[n-l]}e^{\frac{j2\pi\epsilon n}{K}} \end{aligned} \tag{13}$$

Thus, signal (12) goes through GFDM demodulator and the estimated symbol at $k^{'}$-th subcarrier and $m^{'}$-th time-slot is

$$\begin{aligned} \widehat{d}_{k^{'},m^{'}} &= \sum_{n=0}^{MK-1} (r_{CFO}[n])w_{m^{'}}[n]e^{\frac{-j2\pi k^{'}n}{K}} \\ &= U^d_{k,'m'} + U^{d,im}_{k,'m'} + U^s_{k,'m'} + N^{eq}_{k,'m'} \end{aligned} \tag{14}$$

where $w_{m}[n] = w[n - mK]_{MK}$ is circularly shifted version of receiver filter impulse response $w[n]$. Moreover, $U^d_{k,'m'}$ and $U^{d,im}_{k,'m'}$ are corresponding terms for downlink signal and $U^s_{k,'m'}$ is corresponding term to interference signal from U_2 on U_1 . Finally, $N^{eq}_{k,'m'}$ indicates the equivalent noise. All of these terms could be derived by utilizing (12), (13) and (14).

III. Signal Power Analysis

Here, we derive the powers of desired signal, interference signal and noise in both downlink and uplink. We assume two separate up/down conversion oscillators of the base-station. This will result in two separate phase noise processes. Indeed, if there is a physical separation in the transmitter and receiver of base-station, then this model is appropriate. Moreover, single common local oscillator for both up/down conversions has also been considered for compact full-duplex transceivers [24]. However, we do not consider that option in this paper.

A. Uplink Transmission

In this section, the power of the residual SI signal, the power of desired signal, and the power of the equivalent noise are derived.

1) RSI Signal Power: To derive this, we use standard models for the RSI channel and phase noise. We assume that $h_{RSI}[n] = \sum_{l=0}^{L-1} h_{RSI,l}\delta[n-l]$ is a wide-sense stationary uncorrelated scattering (WSSUS) process. WSSUS processes are commonly used for modeling multipath fading channels, e.g., to describe the short-term variations. The WSSUS model allows the channel correlation function to be time-invariant and the paths with different delays to be uncorrelated. These properties have been observed empirically. For this reason, we assume WSSUS processes for all wireless channels in our system. Accordingly, the taps $h_{RSI,l}$ are mutually independent, $\mathbb{E}_h[h_{RSI,l}] = 0$ and $\mathbb{E}_h[|h_{RSI,l}|^2] = \sigma^2_{RSI,l}$, $l = 0, 1, \ldots, L-1$ [24]. Furthermore, Brownian motion free-running oscillators [30] generate phase noise $[\phi[n+1] - \phi[n]] \sim \mathcal{N}(0, 4\pi\beta T_s)$, where $\phi[n]$ is Brownian motion with 3-dB bandwidth of β and T_s is the sample interval. The autocorelation function of $\phi[n]$ may be expressed as

$$\mathbb{E}_\phi\left[e^{j\phi[n_1]}e^{-j\phi[n_2]}\right] = e^{-2|n_1-n_2|\pi\beta T_s}. \tag{15}$$

Moreover, complex data symbols are uncorrelated ($\mathbb{E}_d[d_{k_1,m_1}d^*_{k_2,m_2}] = \delta[k_1-k_2]\delta[m_1-m_2]$). We also assume that the multipath fading channels, transmitted data and phase noise are independent random processes. These assumptions are standard throughout the literature. By utilizing them, we readily find that the variance of the linear residual SI after analog linear cancellation is given by $\sigma^{SI-ALC}_{k,'m'} = \mathbb{E}[|R^{SI}_{k,'m'}|^2] = \mathbb{E}_h[\mathbb{E}_\phi[\mathbb{E}_d[|R^{SI}_{k,'m'}|^2]]]$, which after straightforward manipulation, is derived as

$$\begin{aligned} \sigma^{SI-ALC}_{k,'m'} = &\alpha \sum_{l=0}^{L-1}\sum_{n_1=0}^{MK-1}\sum_{n_2=0}^{MK-1} f_{m'}[n_1]f^*_{m'}[n_2]e^{-4|n_1-n_2|\pi\beta T_s} \\ &\times \left(|g_{TX,d}g_{RX,d}|^2 e^{\frac{j2\pi(n_1-n_2)\epsilon}{K}} + |g_{TX,I}g_{RX,I}|^2 e^{\frac{-j2\pi(n_1-n_2)\epsilon}{K}}\right) \\ &\times \sum_{k=0}^{K-1}\sum_{m=0}^{M-1} \sigma^2_{RSI,l} g_m[n_1-l]g^*_m[n_2-l]e^{\frac{j2\pi(n_1-n_2)(k-k^{'})}{K}}. \end{aligned} \tag{16}$$

The power of the linear residual SI after complementary digital linear cancellation can be defined as $\sigma^{SI-DLC}_{k,'m'} = \mathbb{E}[|R^{SI}_{k,'m'} - R^{DLC}_{k,'m'}|^2]$ which is given by

$$\begin{aligned} \sigma^{SI-DLC}_{k,'m'} = &\alpha \sum_{n_1=0}^{MK-1}\sum_{n_2=0}^{MK-1} f_{m'}[n_1]f^*_{m'}[n_2]e^{-4|n_1-n_2|\pi\beta T_s} \\ &\times \left(|g_{TX,d}g_{RX,d}|^2 e^{\frac{j2\pi(n_1-n_2)\epsilon}{K}} + |g_{TX,I}g_{RX,I}|^2 e^{\frac{-j2\pi(n_1-n_2)\epsilon}{K}}\right) \\ &\times \left\{\left[\sum_{l=0}^{L-1}\sum_{\substack{k=0 \\ k\neq k' \,\&\, m\neq m'}}^{K-1}\sum_{m=0}^{M-1} \sigma^2_{RSI,l} g_m[n_1-l]g^*_m[n_2-l] \right.\right. \\ &\left.\left. \times e^{\frac{j2\pi(n_1-n_2)(k-k^{'})}{K}}\right] + \left[\sigma^2_{ee} g_{m'}[n_1-l]g^*_{m'}[n_2-l]\right]\right\} \end{aligned} \tag{17}$$

where σ^2_{ee} is the channel estimation error variance, which is modeled as $\sigma^2_{ee} = t \times \kappa$ where t and κ indicate analog linear

cancellation and digital linear cancellation suppression, respectively [24]. Note that (16) and (17) depend on multipath profile, 3-dB phase noise bandwidth, normalized CFO, IQ imbalance coefficients, number of subcarriers and time-slots and GFDM receiver and transmitter filters. Thus, all these parameters affect the efficiency of analog and digital SI cancellations. Similarly, the conjugate-residual-SI signal power after analog linear cancellation and after complementary digital linear cancellation could be formulated as

$$\begin{aligned}&\sigma^{SI-im-ALC}_{k,'m'}\\&=\alpha\sum_{l=0}^{L-1}\sum_{n_1=0}^{MK-1}\sum_{n_2=0}^{MK-1} f_{m'}[n_1]f^*_{m'}[n_2]e^{-4|n_1-n_2|\pi\beta T_s}\\&\times\left(|g_{TX,I}g_{RX,d}|^2e^{\frac{j2\pi(n_1-n_2)\epsilon}{K}}+|g_{TX,d}g_{RX,I}|^2e^{\frac{-j2\pi(n_1-n_2)\epsilon}{K}}\right)\\&\times\sum_{k=0}^{K-1}\sum_{m=0}^{M-1}\sigma^2_{RSI,l}g^*_m[n_1-l]g_m[n_2-l]e^{\frac{-j2\pi(n_1-n_2)(k+k')}{K}}\end{aligned}\tag{18}$$

and

$$\begin{aligned}\sigma^{SI-im-DLC}_{k,'m'}&=\alpha\sum_{n_1=0}^{MK-1}\sum_{n_2=0}^{MK-1} f_{m'}[n_1]f^*_{m'}[n_2]e^{-4|n_1-n_2|\pi\beta T_s}\\&\times\left(|g_{TX,I}g_{RX,d}|^2e^{\frac{j2\pi(n_1-n_2)\epsilon}{K}}+|g_{TX,d}g_{RX,I}|^2e^{\frac{-j2\pi(n_1-n_2)\epsilon}{K}}\right)\\&\times\left\{\left[\sum_{l=0}^{L-1}\sum_{\substack{k=0\\k\neq k'\&m\neq m'}}^{K-1}\sum_{m=0}^{M-1}\sigma^2_{RSI,l}g^*_m[n_1-l]g_m[n_2-l]\right.\right.\\&\qquad\left.\times e^{\frac{-j2\pi(n_1-n_2)(k+k')}{K}}\right]\\&\quad\left.+\left[\sigma^2_{ee}g^*_{m'}[n_1-l]g_{m'}[n_2-l]e^{\frac{-j4\pi(n_1-n_2)k'}{K}}\right]\right\}\end{aligned}\tag{19}$$

where $\sigma^{SI-im-ALC}_{k,'m'}=\mathbb{E}[|R^{SI,im}_{k,'m'}|^2]$ and $\sigma^{SI-im-DLC}_{k,'m'}=\mathbb{E}[|R^{SI,im}_{k,'m'}-R^{DLC,i}_{k,'m'}|^2]$. Again, the results depend on multiple system parameters, and hence provide the means and flexibility of system performance evaluations for different configurations. Following (17) and (19), total power of residual SI signal after complementary digital linear cancellation may be expressed as

$$\sigma^{SI}_{k,'m'}=\sigma^{SI-DLC}_{k,'m'}+\sigma^{SI-im-DLC}_{k,'m'}.\tag{20}$$

2) Desired Uplink Signal Power: By substituting $k=k'$ and $m=m'$, the desired symbol could be extracted from $R^s_{k,'m'}$ as

$$d^{s-up}_{k,'m'}=\sqrt{\alpha_s}d^s_{k,'m'}\sum_{l=0}^{L-1}\sum_{n=0}^{MK-1}h^I_2[n,l]f_{m'}[n]g_{m'}[n-l]e^{\frac{-j2\pi k'l}{K}}.\tag{21}$$

Thus, from (21), interference signal could be expressed as $R^{ss}_{k,'m'}=R^s_{k,'m'}-d^{s-up}_{k,'m'}$. We assume a WSSUS uplink channel $h_2[n]=\sum_{l=0}^{L-1}h_{2,l}\delta[n-l]$. Thus $h_{2,l}$ are mutually independent, $\mathbb{E}[h_{2,l}]=0$ and $\mathbb{E}[|h_{2,l}|^2]=\sigma^2_{2,l},\ l=0,1,\ldots,L-1$. Therefore, the variance of the desired symbol could be expressed as

$$\begin{aligned}\sigma^s_{k,'m'}&=\mathbb{E}\left[|d^{s-up}_{k,'m'}|^2\right]=\alpha_s|g_{RX,d}|^2\sum_{l=0}^{L-1}\sum_{n_1=0}^{MK-1}\sum_{n_2=0}^{MK-1}\sigma^2_{2,l}\\&e^{-2|n_1-n_2|\pi\beta T_s}f_{m'}[n_1]f^*_{m'}[n_2]g_{m'}[n_1-l]g^*_{m'}[n_2-l]e^{\frac{j2\pi(n_1-n_2)\epsilon}{K}}.\end{aligned}\tag{22}$$

The interference signals could be considered as $R^{ss}_{k,'m'}$ and $R^{s,im}_{k,'m'}$. The variance of the first-term could be calculated as

$$\begin{aligned}\sigma^{R^{ss}}_{k,'m'}&=\mathbb{E}\left[|R^s_{k,'m'}-d^{s-up}_{k,'m'}|^2\right]=\mathbb{E}\left[|R^s_{k,'m'}|^2\right]+\mathbb{E}\left[|d^{s-up}_{k,'m'}|^2\right]\\&-2\text{real}\left(\mathbb{E}\left[R^{*s}_{k,'m'}d^{s-up}_{k,'m'}\right]\right)=\mathbb{E}\left[|R^s_{k,'m'}|^2\right]+\mathbb{E}\left[|d^{s-up}_{k,'m'}|^2\right]\\&-2\mathbb{E}\left[|d^{s-up}_{k,'m'}|^2\right]=\sigma^{R^s}_{k,'m'}-\sigma^s_{k,'m'}\end{aligned}\tag{23}$$

where $\sigma^{R^s}_{k,'m'}=\mathbb{E}[|R^s_{k,'m'}|^2]$ is equal to

$$\begin{aligned}\sigma^{R^s}_{k,'m'}&=\alpha_s|g_{RX,d}|^2\sum_{l=0}^{L-1}\sum_{n_1=0}^{MK-1}\sum_{n_2=0}^{MK-1}\sum_{k=0}^{K-1}\sum_{m=0}^{M-1}\sigma^2_{2,l}e^{-2|n_1-n_2|\pi\beta T_s}\\&\times f_{m'}[n_1]f^*_{m'}[n_2]g_m[n_1-l]g^*_m[n_2-l]e^{\frac{j2\pi(n_1-n_2)(\epsilon+k-k')}{K}}.\end{aligned}\tag{24}$$

Moreover, the variance of the second term could be expressed as

$$\begin{aligned}\sigma^{R^{s,im}}_{k,'m'}&=\alpha_s|g_{RX,I}|^2\sum_{l=0}^{L-1}\sum_{n_1=0}^{MK-1}\sum_{n_2=0}^{MK-1}\sum_{k=0}^{K-1}\sum_{m=0}^{M-1}\sigma^2_{2,l}e^{-2|n_1-n_2|\pi\beta T_s}\\&\times f_{m'}[n_1]f^*_{m'}[n_2]g^*_m[n_1-l]g_m[n_2-l]e^{\frac{-j2\pi(n_1-n_2)(\epsilon+k+k')}{K}}.\end{aligned}\tag{25}$$

Obviously, derived results are function of system parameters including amount of phase noise, CFO, IQ imbalance, channel propagation and GFDM parameters. The total power of the interference signal is given by

$$\sigma^{s,i}_{k,'m'}=\sigma^{R^s}_{k,'m'}+\sigma^{R^{s,im}}_{k,'m'}-\sigma^s_{k,'m'}.\tag{26}$$

3) Equivalent Noise Power: Since additive Gaussian noise is $\mathcal{CN}(0,N_0)$, the variance of direct equivalent noise $w^{eq}_{k,'m'}$ in (9) is given by

$$\sigma^{w^{eq}}_{k,'m'}=\mathbb{E}\left[|w^{eq}_{k,'m'}|^2\right]=|g_{RX,d}|^2N_0\sum_{n=0}^{MK-1}|f_{m'}[n]|^2.\tag{27}$$

Similarly, the power of image equivalent noise $w^{eq,im}_{k,'m'}$ in (9) is written as

$$\sigma^{w^{eq,im}}_{k,'m'}=\mathbb{E}\left[|w^{eq,im}_{k,'m'}|^2\right]=|g_{RX,I}|^2N_0\sum_{n=0}^{MK-1}|f_{m'}[n]|^2.\tag{28}$$

According to (27) and (28), noise power depends on IQ coefficient, noise variance and the receiver filter. Moreover, they are independent of subcarrier index. Finally, the total noise

power can be written as

$$\sigma^{w}_{k,'m'} = \sigma^{w^{eq}}_{k,'m'} + \sigma^{w^{eq,im}}_{k,'m'}. \tag{29}$$

B. Downlink Transmission

Here, the power of the downlink signal and interference signal between the two users and noise are derived in closed-form. According to the WSSUS model for downlink channel $h_1[n] = \sum_{l=0}^{L-1} h_1[l]\delta[n-l]$, $h_{1,l}$ are mutually independent, $\mathbb{E}[h_{1,l}] = 0$ and $\mathbb{E}[|h_{1,l}|^2] = \sigma^2_{1,l}$, $l = 0, 1, \ldots, L-1$.

1) Desired Downlink Signal Power: According to (14), desired downlink symbol can be extracted from $U^d_{m,'k'}$ by substituting $k = k'$ and $m = m'$ as

$$d^{s-down}_{k,'m'} = \sqrt{\alpha} d_{k,'m'} \sum_{l=0}^{L-1} \sum_{n=0}^{MK-1} h^I_1[n,l] w_{m'}[n] g_{m'}[n-l] e^{\frac{-j2\pi k' l}{K}}. \tag{30}$$

The variance of the desired downlink symbol is thus written as

$$\sigma^d_{k,'m'} = \mathbb{E}\left[|d^{s-down}_{k,'m'}|^2\right] = \alpha |g_{TX,d}|^2 \sum_{l=0}^{L-1} \sum_{n_1=0}^{MK-1} \sum_{n_2=0}^{MK-1} \sigma^2_{1,l}$$

$$e^{-2|n_1-n_2|\pi\beta T_s} w_{m'}[n_1] w^*_{m'}[n_2] g_{m'}[n_1-l] g^*_{m'}[n_2-l] e^{\frac{j2\pi(n_1-n_2)\epsilon}{K}}. \tag{31}$$

Now by subtracting the desired downlink symbol in (30), interference signals may be considered as $U^d_{k,'m'} - d^{s-down}_{k,'m'}$ and $U^{d,im}_{k,'m'}$. Similar to (23) and according to (12), (13) and (14), the variance of the first term could be calculated as $\sigma^{U^d}_{k,'m'} - \sigma^d_{k,'m'}$ where $\sigma^{U^d}_{k,'m'} = \mathbb{E}[|U^d_{k,'m'}|^2]$ is given by

$$\sigma^{U^d}_{k,'m'} = \alpha |g_{TX,d}|^2 \sum_{l=0}^{L-1} \sum_{n_1=0}^{MK-1} \sum_{n_2=0}^{MK-1} \sum_{k=0}^{K-1} \sum_{m=0}^{M-1} \sigma^2_{1,l} e^{-2|n_1-n_2|\pi\beta T_s}$$

$$\times\, w_{m'}[n_1] w^*_{m'}[n_2] g_m[n_1-l] g^*_m[n_2-l] e^{\frac{j2\pi(n_1-n_2)(\epsilon+k-k')}{K}}. \tag{32}$$

Furthermore, the variance of the second term is given by

$$\sigma^{U^{d,im}}_{k,'m'} = \alpha |g_{TX,I}|^2 \sum_{l=0}^{L-1} \sum_{n_1=0}^{MK-1} \sum_{n_2=0}^{MK-1} \sum_{k=0}^{K-1} \sum_{m=0}^{M-1} \sigma^2_{1,l} e^{-2|n_1-n_2|\pi\beta T_s}$$

$$\times\, w_{m'}[n_1] w^*_{m'}[n_2] g^*_m[n_1-l] g_m[n_2-l] e^{\frac{j2\pi(n_1-n_2)(\epsilon-k-k')}{K}}. \tag{33}$$

Thus, the total power of the interference signal is given by

$$\sigma^{d-i}_{k,'m'} = \sigma^{U^d}_{k,'m'} + \sigma^{U^{d,im}}_{k,'m'} - \sigma^d_{k,'m'}. \tag{34}$$

The results clearly show that power of different components of desired downlink signal are dependent of phase 3-dB phase noise bandwidth, CFO parameter, IQ imbalance coefficients, multipath profile of channels and GFDM parameters.

2) Co-Channel Interference Signal Power: We again assume the WSSUS model for co-channel interference channel between the uplink user and the downlink user, which is expressed as $h_3[n] = \sum_{l=0}^{L-1} h_{3,l}\delta[n-l]$. Thus, the taps $h_{3,l}$ are mutually independent, $\mathbb{E}[h_{3,l}] = 0$ and $\mathbb{E}[|h_{3,l}|^2] = \sigma^2_{3,l}$, $l = 0, 1, \ldots, L-1$. Following (12), (13) and (14), the variance of the interference signal from U_2 onto U_1 can be expressed as

$$\sigma^{U^s}_{k,'m'} = \alpha_s \sum_{l=0}^{L-1} \sum_{n_1=0}^{MK-1} \sum_{n_2=0}^{MK-1} \sum_{k=0}^{K-1} \sum_{m=0}^{M-1} \sigma^2_{3,l} w_{m'}[n_1] w^*_{m'}[n_2]$$

$$\times\, g_m[n_1-l] g^*_m[n_2-l] e^{\frac{j2\pi(n_1-n_2)(\epsilon+k-k')}{K}}. \tag{35}$$

This co-channel interference (35) is a function of multipath profile of channel between the two users, the normalized CFO and the transmit and receive filters of GFDM.

3) Equivalent Noise Power: Since additive noise is distributed as $\mathcal{N}(0, N_0)$, the variance of equivalent noise in (14) may be expressed as

$$\sigma^{N^{eq}}_{k,'m'} = \mathbb{E}\left[|N^{eq}_{k,'m'}|^2\right] = N_0 \sum_{n=0}^{MK-1} |w_{m'}[n]|^2. \tag{36}$$

Similar to the case of uplink transmission, the power of equivalent noise depends on the variance of noise and summation of the receiver filter coefficients and is independent of the index of the subcarrier.

IV. SIR Formulation and Filter Optimization

Here, SIRs for both downlink and uplink are derived, and SIR-maximizing optimal receiver filters for base-station and U_1 are proposed.

A. Uplink Transmission

From (20), (22) and (26), SIR of the estimated symbol in k'-th subcarrier and m'-th subsymbol is written as

$$\Gamma^{up}_{k,'m'} = \frac{\sigma^s_{k,'m'}}{\sigma^{SI}_{k,'m'} + \sigma^{s,i}_{k,'m'}}. \tag{37}$$

Since GFDM uses non-orthogonal waveforms, it performs worse than OFDM in the presence of RF impairments. This suggests that it should achieve lower SIR than OFDM. Fortunately, the performance of GFDM can be improved by exploiting the degrees of freedom inherent in receiver prototype filter $\{f[n]\}$. However, the SIR depends on both transmit and receive filter prototypes ($g[n]$ and $f[n]$). To retain the benefits of GFDM such as lower out-of-band emissions, we fix $g[n]$ to be a conventional filter of raised cosine type.

Following that, we can optimize receiver filter $\{f[n]\}$ to maximize the SIR given RF impairments. Let us denote $\mathbf{f_{k,'m'}} = \mathbf{S}_{k'}\mathbf{M}_{m'M}\mathbf{f}_{0,0} \in \mathbb{C}^{MK\times 1}$ contains samples of $f_{k,'m'}[n] = f_{m'}[n] e^{\frac{-j2\pi k' n}{K}}$ in (8) where $\mathbf{f}_{0,0} \in \mathbb{C}^{MK\times 1}$ is the column vector including receiver filter $f[n]$ samples, $\mathbf{M}_{m'M} \in \mathbb{C}^{MK\times MK}$ circularly shifts $\mathbf{f}_{0,0}$ and $\mathbf{S}_{k'} = \text{diag}([1, e^{\frac{-j2\pi k'}{K}}, \ldots, e^{\frac{-j2\pi k'(MK-1)}{K}}]) \in \mathbb{C}^{MK\times MK}$ is the subcarrier mapping matrix. It is worth mentioning that (8) could be expressed as $\hat{d}^s_{k,'m'} = \mathbf{y}_{IQ}\mathbf{f}_{k,'m'}$ where $\mathbf{y}_{IQ} \in \mathbb{C}^{1\times MK}$ contains $y_{IQ}[n]$. Moreover, according to derivations, we rewrite the derived variances in matrix form as $\sigma^s_{k,'m'} = \alpha_s \mathbf{f}^H_{k,'m'} \mathbf{V}^s_{k,'m'} \mathbf{f}_{k,'m'}$, $\sigma^{SI}_{k,'m'} = \alpha \mathbf{f}^H_{k,'m'} \mathbf{V}^{SI} \mathbf{f}_{k,'m'}$ and

$\sigma^{s,i}_{k,'m'} = \alpha_s(\mathbf{f}^H_{k,'m'}\mathbf{V}^R\mathbf{f}_{k,'m'} - \mathbf{f}^H_{k,'m'}\mathbf{V}^s_{k,'m'}\mathbf{f}_{k,'m'})$ where

$$V^s_{k,'m'}[n_2,n_1] = \sum_{l=0}^{L-1} |g_{RX,d}|^2\sigma^2_{2,l}e^{-2|n_1-n_2|\pi\beta T_s}g_{m'}[n_1-l] \times g^*_{m'}[n_2-l]e^{\frac{j2\pi(n_1-n_2)(\epsilon+k')}{K}}. \quad (38)$$

$$\begin{aligned} V^{SI}[n_2,n_1] &= e^{-4|n_1-n_2|\pi\beta T_s}\left\{\left[\sum_{l=0}^{L-1}\sum_{\substack{k=0\\k\neq k'\&m\neq m'}}^{K-1}\sum_{m=0}^{M-1}\sigma^2_{RSI,l}g_m[n_1-l]\right.\right. \\ &\times g^*_m[n_2-l]\Big(|g_{TX,d}g_{RX,d}|^2e^{\frac{j2\pi(n_1-n_2)(\epsilon+k)}{K}} \\ &+|g_{TX,I}g_{RX,I}|^2e^{\frac{-j2\pi(n_1-n_2)(\epsilon-k)}{K}}+|g_{TX,I}g_{RX,d}|^2 \\ &\left.\left.\times e^{\frac{j2\pi(n_1-n_2)(\epsilon-k)}{K}}+|g_{TX,d}g_{RX,I}|^2e^{\frac{-j2\pi(n_1-n_2)(\epsilon+k)}{K}}\Big)\right] \\ &+\left[\sigma^2_{ee}g_{m'}[n_1-l]g^*_{m'}[n_2-l]\Big(|g_{TX,d}g_{RX,d}|^2\right. \\ &\times e^{\frac{j2\pi(n_1-n_2)(\epsilon+k')}{K}}+|g_{TX,I}g_{RX,I}|^2e^{\frac{-j2\pi(n_1-n_2)(\epsilon-k')}{K}} \\ &+|g_{TX,I}g_{RX,d}|^2e^{\frac{j2\pi(n_1-n_2)(\epsilon-k')}{K}} \\ &\left.\left.+|g_{TX,d}g_{RX,I}|^2e^{\frac{-j2\pi(n_1-n_2)(\epsilon+k')}{K}}\Big)\right]\right\} \end{aligned} \quad (39)$$

$$\begin{aligned} V^R[n_2,n_1] &= \sum_{l=0}^{L-1}\sum_{k=0}^{K-1}\sum_{m=0}^{M-1}\sigma^2_{2,l}g_m[n_1-l]g^*_m[n_2-l] \\ &\times e^{-2|n_1-n_2|\pi\beta T_s}\Big(|g_{RX,d}|^2e^{\frac{j2\pi(n_1-n_2)(\epsilon+k)}{K}}+|g_{RX,I}|^2 \\ &\times e^{\frac{-j2\pi(n_1-n_2)(\epsilon+k)}{K}}\Big). \end{aligned} \quad (40)$$

Now, in order to find $\mathbf{f}_{0,0}$ that maximizes SIR, we rewrite SIR in matrix form as

$$\begin{aligned} \Gamma^{up} &= \frac{\alpha_s\sum_{k'=0}^{K-1}\sum_{m'=0}^{M-1}\mathbf{f}^H_{k,'m'}\mathbf{V}^s_{k,'m'}\mathbf{f}_{k,'m'}}{\sum_{k'=0}^{K-1}\sum_{m'=0}^{M-1}\mathbf{f}^H_{k,'m'}\mathbf{V}\mathbf{f}_{k,'m'}-\alpha_s\mathbf{f}^H_{k,'m'}\mathbf{V}^s_{k,'m'}\mathbf{f}_{k,'m'}} \\ &= \frac{\mathbf{f}^H_{0,0}\mathbf{T}_1\mathbf{f}_{0,0}}{\mathbf{f}^H_{0,0}(\mathbf{T}_2-\mathbf{T}_1)\mathbf{f}_{0,0}} \end{aligned} \quad (41)$$

where $\mathbf{V} = \alpha\mathbf{V}^{SI}+\alpha_s\mathbf{V}^R$, $\mathbf{T}_1 = \alpha_s\sum_{k'=0}^{K-1}\sum_{m'=0}^{M-1}\mathbf{M}^H_{m'M}\mathbf{S}^H_{k'}\mathbf{V}^s_{k,'m'}\mathbf{S}_{k'}\mathbf{M}_{m'M}$ and $\mathbf{T}_2 = \sum_{k'=0}^{K-1}\sum_{m'=0}^{M-1}\mathbf{M}^H_{m'M}\mathbf{S}^H_{k'}\mathbf{V}\mathbf{S}_{k'}\mathbf{M}_{m'M}$. Therefore, the filter design problem for maximizing the SIR could be formulated as

$$\begin{aligned} \mathbf{f}^{opt}_{0,0} &= \arg\ \max_{\mathbf{x}}\ \frac{\mathbf{x}^H\mathbf{T}_1\mathbf{x}}{\mathbf{x}^H(\mathbf{T}_2-\mathbf{T}_1)\mathbf{x}} \\ &\text{s.t.}\quad ||\mathbf{x}||^2 = 1 \end{aligned} \quad (42)$$

where $\mathbf{x}\in\mathbb{C}^{MK\times 1}$ and $||\mathbf{x}||$ indicates norm of $\mathbf{x}$. To solve this, we first consider the Cholesky factorization as $\mathbf{T}_2-\mathbf{T}_1 = \mathbf{L}\mathbf{L}^H$. This can be substituted in (42) to yield

$$\frac{\mathbf{x}^H\mathbf{T}_1\mathbf{x}}{\mathbf{x}^H(\mathbf{T}_2-\mathbf{T}_1)\mathbf{x}} = \frac{\mathbf{x}^H\mathbf{T}_1\mathbf{x}}{\mathbf{x}^H(\mathbf{L}\mathbf{L}^H)\mathbf{x}} = \frac{\mathbf{y}^H\mathbf{L}^{-1}\mathbf{T}_1\mathbf{L}^{H-1}\mathbf{y}}{\mathbf{y}^H\mathbf{y}}$$

where $\mathbf{y} = \mathbf{L}^H\mathbf{x}$. The above ratio is known as Rayleigh quotient [37]. It can be readily shown that the Rayleigh quotient reaches its maximum value when $\mathbf{y}$ is the corresponding eigenvector of the maximum eigenvalue of $\mathbf{L}^{-1}\mathbf{T}_1\mathbf{L}^{H-1}$. But, this eigenvalue remains the same if $\mathbf{L}^{H-1}\mathbf{L}^{-1}\mathbf{T}_1 = (\mathbf{T}_2-\mathbf{T}_1)^{-1}\mathbf{T}_1$. Therefore, the optimal receiver filter is given by [38]

$$\mathbf{f}^{opt}_{0,0} \propto \max\left[\text{eigenvector}\left((\mathbf{T}_2-\mathbf{T}_1)^{-1}\mathbf{T}_1\right)\right]. \quad (43)$$

Thus, this optimal receiver filter maximizes the SIR of the GFDM full-duplex under the RF impairments after analog linear cancellation and complementary digital linear cancellation.

B. Downlink Transmission

Due to the full duplex operation of the base-station, uplink and downlink transmissions occupy same frequency and time slots. Thus, interference from U_2 in uplink on U_1 in downlink decreases the performance of the downlink. In the uplink section, we have proposed the SIR-maximizing receiver filter. However, with two stage SI cancellations, residual SI as a main source of interference on the desired uplink signal is eliminated. But since there is no interference cancellation in downlink, receiver filter design alleviates the effects of interference signal from other user. By utilizing (32), (33) and (35), SIR for the k'-th subcarrier and m'-th subsymbol can be expressed as

$$\Gamma^{down}_{k,'m'} = \frac{\sigma^d_{k,'m'}}{\sigma^{d-i}_{k,'m'}+\sigma^{Us}_{k,'m'}}. \quad (44)$$

Similar to the uplink case, we rewrite the variance terms in (44) as a function of the receiver filter. Let us denote $\mathbf{w_{k,'m'}} = \mathbf{S}_{k'}\mathbf{M}_{m'M}\mathbf{w}_{0,0}\in\mathbb{C}^{MK\times 1}$ where $\mathbf{w}_{0,0}\in\mathbb{C}^{MK\times 1}$ is the column vector including receiver filter $w[n]$ samples. The variances could be expressed in matrix form as $\sigma^d_{k,'m'} = \alpha\mathbf{w}^H_{k,'m'}\boldsymbol{\eta}^d_{k,'m'}\mathbf{w}_{k,'m'}$, $\sigma^{U^s}_{k,'m'} = \alpha_s\mathbf{w}^H_{k,'m'}\boldsymbol{\eta}^s\mathbf{w}_{k,'m'}$ and $\sigma^{d-i}_{k,'m'} = \alpha(\mathbf{w}^H_{k,'m'}\boldsymbol{\eta}^{d,i}\mathbf{f}_{k,'m'} - \mathbf{w}^H_{k,'m'}\boldsymbol{\eta}^d_{k,'m'}\mathbf{w}_{k,'m'})$ where

$$\eta^d_{k,'m'}[n_2,n_1] = \sum_{l=0}^{L-1}|g_{TX,d}|^2\sigma^2_{1,l}e^{-2|n_1-n_2|\pi\beta T_s}g_{m'}[n_1-l] \times g^*_{m'}[n_2-l]e^{\frac{j2\pi(n_1-n_2)(\epsilon+k')}{K}}, \quad (45)$$

$$\eta^s[n_2,n_1] = \sum_{l=0}^{L-1}\sum_{k=0}^{K-1}\sum_{m=0}^{M-1}\sigma^2_{3,l}g_m[n_1-l]g^*_m[n_2-l]e^{\frac{j2\pi(n_1-n_2)(\epsilon+k)}{K}}, \quad (46)$$

and

$$\eta_{m'}^{d-i}[n_2,n_1]=\sum_{l=0}^{L-1}\sum_{k=0}^{K-1}\sum_{m=0}^{M-1}\sigma_{1,l}^2 g_m[n_1-l]g_m^*[n_2-l] \times e^{-2|n_1-n_2|\pi\beta T_s}\Big(|g_{TX,d}|^2 e^{\frac{j2\pi(n_1-n_2)(\epsilon+k)}{K}} + |g_{TX,I}|^2 e^{\frac{j2\pi(n_1-n_2)(\epsilon-k)}{K}}\Big). \quad (47)$$

By utilizing (45), (47) and (46), we can write the SIR of the downlink transmission as

$$\Gamma^{down} = \frac{\alpha\sum_{k'=0}^{K-1}\sum_{m'=0}^{M-1}\mathbf{w}_{k,'m'}^H\boldsymbol{\eta}_{k,'m'}^d\mathbf{w}_{k,'m'}}{\sum_{k'=0}^{K-1}\sum_{m'=0}^{M-1}\mathbf{w}_{k,'m'}^H\boldsymbol{\eta}^T\mathbf{w}_{k,'m'}-\alpha\mathbf{w}_{k,'m'}^H\boldsymbol{\eta}_{k,'m'}^d\mathbf{w}_{k,'m'}} = \frac{\mathbf{w}_{0,0}^H\mathbf{T}_3\mathbf{w}_{0,0}}{\mathbf{w}_{0,0}^H(\mathbf{T}_4-\mathbf{T}_3)\mathbf{w}_{0,0}} \quad (48)$$

where $\boldsymbol{\eta}^T=\alpha_s\boldsymbol{\eta}^s+\alpha\boldsymbol{\eta}^{d-i}$, $\mathbf{T}_3=\alpha\sum_{k'=0}^{K-1}\sum_{m'=0}^{M-1}\mathbf{M}_{m'M}^H\mathbf{S}_{k'}^H\boldsymbol{\eta}_{k,'m'}^d\mathbf{S}_{k'}\mathbf{M}_{m'M}$ and $\mathbf{T}_4=\sum_{k'=0}^{K-1}\sum_{m'=0}^{M-1}\mathbf{M}_{m'M}^H\mathbf{S}_{k'}^H\boldsymbol{\eta}^T\mathbf{S}_{k'}\mathbf{M}_{m'M}$. Following (42) and (48), optimal uplink receiver filter is given by

$$\mathbf{w}_{0,0}^{opt}\propto\max\left[\text{eigenvector}\left((\mathbf{T}_4-\mathbf{T}_3)^{-1}\mathbf{T}_3\right)\right]. \quad (49)$$

V. Achievable Rate Region

Rate region refers to the ordered pair of the downlink data rate and uplink data rate. These two are mutually dependent because the transmit powers affect both SI and co-channel interference. The rate region can be obtained by maximizing the uplink rate under the constraint of constant downlink rate.

Here, we express both downlink and uplink rates and formulate their rates as optimization problems. By using residual SI power after complementary digital linear cancellation (20), desired signal (22) and equivalent thermal noise (29) for uplink in Section III-A, and Similarly, according to derived expressions (31)–(36) for downlink in Section III-B, signal-to-interference-plus-noise ratio (SINR) of uplink and downlink can be formulated as

$$\Upsilon_{k,'m'}^{up}=\frac{\sigma_{k,'m'}^s}{\sigma_{k,'m'}^{SI}+\sigma_{k,'m'}^{s,i}+\sigma_{k,'m'}^w}=\frac{\alpha_s A_{k,'m'}^{up}}{\alpha_s B_{k,'m'}^{up}+\alpha C_{k,'m'}^{up}+D_{k,'m'}^{up}}$$

$$\Upsilon_{k,'m'}^{down}=\frac{\sigma_{k,'m'}^d}{\sigma_{k,'m'}^{d-i}+\sigma_{k,'m'}^{U^s}+\sigma_{k,'m'}^{N^{eq}}}=\frac{\alpha A_{k,'m'}^{down}}{\alpha B_{k,'m'}^{down}+\alpha_s C_{k,'m'}^{down}+D_{k,'m'}^{down}} \quad (50)$$

where $A_{k,'m'}^{up}=\mathbf{f}_{k,'m'}^H\mathbf{V}_{k,'m'}^s\mathbf{f}_{k,'m'}$, $B_{k,'m'}^{up}=\mathbf{f}_{k,'m'}^H(\mathbf{V}^R-\mathbf{V}_{k,'m'}^s)\mathbf{f}_{k,'m'}$, $C_{k,'m'}^{up}=\mathbf{f}_{k,'m'}^H\mathbf{V}^{SI}\mathbf{f}_{k,'m'}$, $D^{up}=\sigma_{k,'m'}^w$, $A_{k,'m'}^{down}=\mathbf{w}_{k,'m'}^H\boldsymbol{\eta}_{k,'m'}^d\mathbf{w}_{k,'m'}$, $B_{k,'m'}^{down}=\mathbf{w}_{k,'m'}^H(\boldsymbol{\eta}^{d-i}-\boldsymbol{\eta}_{k,'m'}^d)\mathbf{w}_{k,'m'}$, $C_{k,'m'}^{down}=\mathbf{w}_{k,'m'}^H\boldsymbol{\eta}^s\mathbf{w}_{k,'m'}$ and $D^{down}=\sigma_{k,'m'}^{N^{eq}}$. According to (50), the uplink and downlink achievable rates may be expressed as

$$R^{up}(\alpha,\alpha_s)=\sum_{k'=0}^{K-1}\sum_{m'=0}^{M-1}\log_2\left(1+\Upsilon_{k,'m'}^{up}\right)$$

$$R^{down}(\alpha,\alpha_s)=\sum_{k'=0}^{K-1}\sum_{m'=0}^{M-1}\log_2\left(1+\Upsilon_{k,'m'}^{down}\right). \quad (51)$$

Note that both uplink and downlink rates are dependent of system parameters, and different configurations could be considered for evaluating their performance.

Following (51), the optimized rate region is formulated as

$$\max_{\alpha,\alpha_s} R^{up}(\alpha,\alpha_s) \quad (52a)$$

$$\text{s.t. } R^{down}(\alpha,\alpha_s)=R_c \quad (52b)$$

$$\alpha\le P_{\max},\alpha_s\le P_{\max} \quad (52c)$$

where R_c is a constant and P_{max} indicates maximum allowable power that can be consumed in uplink and downlink transmissions. The problem (52) is not convex in general because the objective function $R^{up}(\alpha,\alpha_s)$ is the logarithm of a rational function. However, it can be solved optimally by utilizing the following property.

Proposition 1: Given the target rate constraint $R^{down}(\alpha,\alpha_s)=R_c$, $R^{up}(\alpha,\alpha_s)$ is monotonically increasing over α_s. Thus, the optimization problem (52) is equivalent to maximizing α_s under the same constraints. Define $R_{th}=R^{down}(P_{max},P_{max})$ as the threshold rate. The solution of equivalent problem is equal to $\alpha_s^{opt}=P_{max}$ when $R_c\le R_{th}$ and otherwise is $\alpha^{opt}=P_{max}$.

Proof: See Appendix A. ■

We exploit Proposition 1 to develop Algorithm 1, which deploys the bisection method to optimally solve (52).

Algorithm 1: Maximum Uplink Rate for a Downlink Target Rate.

1: Set maximum allowable power $P_{\max}$.
2: Compute $R_{th}=R^{down}(P_{\max},P_{\max})$ using (51).
3: If $R_c\le R_{th}$, set $\alpha^{opt}=P_{\max}$ and find $\alpha_s^{opt}=P_{\max}$ via bisection method until $R^{down}(\alpha,\alpha_s)=R_c$ and stop.
4: If $R_c>R_{th}$, set $\alpha_s^{opt}=P_{\max}$ and find $\alpha^{opt}=P_{\max}$ via bisection method until $R^{down}(\alpha,\alpha_s)=R_c$ and stop.

VI. Simulation Results

Here, the derived uplink and downlink expressions are verified with simulation results. Moreover, GFDM full-duplex and OFDM are both evaluated and compared in the presence of phase noise, CFO and IQ imbalance. We emphasize that our derivations make no restrictive assumptions on 3-dB phase noise bandwidth, normalized CFO, IRR, GFDM parameters and the channel delay profile. In other words, the derived results are valid for arbitrary scenarios. However, we now assume the following

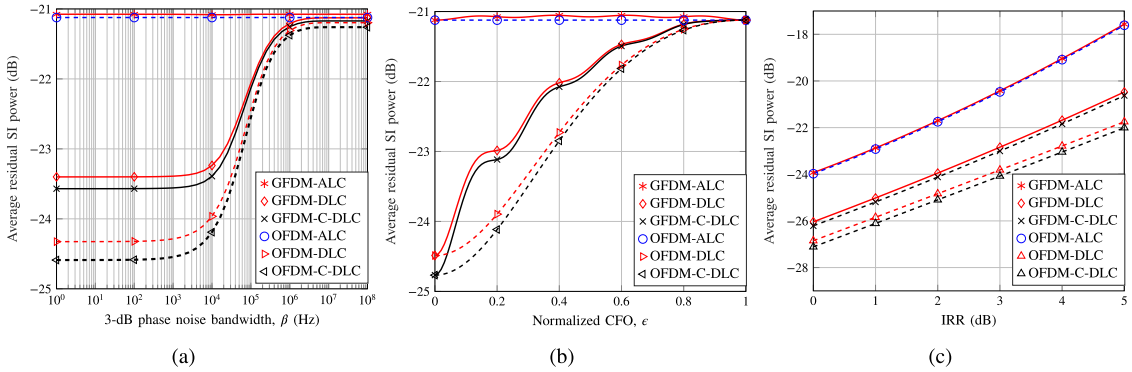

Fig. 2. Average residual SI power versus 3-dB phase noise bandwidth, normalized CFO and IRR.

specific parameter values. For both GFDM and OFDM, the cyclic prefix is equal to the length of the channel, and the number of subcarriers is 32. Additionally, GFDM uses $M = 5$ time slots and a root raised-cosine filter with the roll-off factor 0.1. Sampling frequency is equal to 15.36 MHz [24]. Each wireless channel has five ($L = 5$) independent Rayleigh fading taps. The power delay profile of SI channel in [24] is utilized which is -30 dB, -65 dB, -70 dB and -75 dB for delays of 0, 1, 2 and 4 samples. Note that 30 dB antenna separation results in -30 dB attenuation of the main tap. Without loss of generality, we assume that SI channel $h_{SI}[n]$ is 10 dB stronger than interference channel between two users $h_3[n]$. The multipath downlink channel between base-station transmitter and U_1 has power profile of $[-30, -55, -60, -65, -70]$ dBs. Moreover, we assume that downlink channel $h_1[n]$ is 20 dB stronger than uplink $h_2[n]$ channel. The same IQ imbalance level, $\text{IRR}_{Tx} = \text{IRR}_{Rx}$, is considered for both transmitter and receiver. We assume 30 dB and 50 dB analog and digital SI cancellations, respectively. Therefore, effective channel estimation error variance is equal to 80 dB. Furthermore, the noise variance is -60 dB, and the maximum allowable power is -10 dB. The theoretical results are shown with dash lines.

A. Conventional Receive Filters

Conventional matched filter and zero forcing are two widely used GFDM receiver structures. They have some implementation advantages, but their performance falls short of that of the optimal receive filters. Therefore, it is important to compare them against the derived optimal filters (43) and (49). One frame of GFDM signal in (1) can be written as $\vec{x} = \sqrt{\alpha}\mathbf{d}\mathbf{A}$, where $\mathbf{d} \in \mathbb{C}^{1\times MK}$ is the data vector and $\mathbf{A} \in \mathbb{C}^{MK\times MK}$ is a modulation matrix given by $[\mathbf{A}]_{kM+m,n} = g_m[n]e^{j2\pi n\frac{k}{K}}$. Accordingly, the receiver matrix for matched filter and zero forcing receivers are written as $\mathbf{A}^H$ and $\mathbf{A}^{-1}$, respectively. Furthermore, matched filter and zero forcing receiver filters, $\mathbf{f}_{0,0}^{MF} \in \mathbb{C}^{MK\times 1}$ and $\mathbf{f}_{0,0}^{ZF} \in \mathbb{C}^{MK\times 1}$, are equal to first column of the receiver matrix $\mathbf{A}^H$ and $\mathbf{A}^{-1}$, respectively.

B. Full-Duplex OFDM Results

GFDM is a general form of OFDM. Thus, in the signal model (1), by setting number of time-slots is equal to one, $M = 1$, and prototype filter $g[n]$ is equal to rectangular pulse shape, we get OFDM. Therefore, all the derived expressions can also be used for full-duplex OFDM.

C. SI Signal Power

We next verify our residual SI power analysis (20) by simulation results. Moreover, the comparative OFDM results are also shown. GFDM with zero-forcing receiver (legend GFDM-ZF) with $\alpha = 0$ dB is assumed.

In Fig. 2, average residual SI is plotted versus the 3-dB phase noise bandwidth, normalized CFO and IQ imbalance for GFDM-ZF. Solid and dashed lines represent GFDM and OFDM, respectively. There are five markers per each line. These represent the simulated points. For clarity, more simulation points are not shown. We consider GFDM with analog linear cancellation (legend GFDM-ALC) in (16) and (18). Moreover, we consider GFDM with both digital linear cancellation and complementary digital linear cancellation (legends GFDM-DLC and GFDM-C-DLC) in (17) and (19).

First of all, the simulation results fully match the derived residual SI power. This match points to an independent verification of the validity of our derivations.

This figure also alludes to how the three cancellation techniques will be affected the RF impairments. We observe that C-DLC is slightly more effective than DLC. The former employs conjugate residual SI cancellation, which improves the performance significantly. We also note that ALC achieves the worst performance among the three techniques.

In Fig. 2a, for fixed values of CFO $\epsilon = 0.1$ and 2.5 dB IQ imbalance, residual SI is plotted as a function of phase noise β. This figure depicts the effects of phase noise on the performance of the three SI cancellation techniques. For instance, the performance of ALC is not sensitive to a phase noise increase. However, the situation is different for both DLC and C-DLC. For the range $1 \leq \beta \leq 10^4$, both remain roughly constant regardless of β, but their performance degrades beyond that. However, this limit is less than that of ALC.

In Fig. 2b, we set phase noise at 10 Hz and IQ imbalance at 2.5 dB and change CFO ϵ. This figure depicts the effects of CFO on the performance of the SI cancellation techniques. With increasing ϵ, the residual SI power after either DLC or C-DLC increases and approaches that after ALC. According to (16)–(19), 3-dB phase noise bandwidth, β, and normalized CFO, ϵ, appear in the exponential terms, and the trends in Fig. 2a

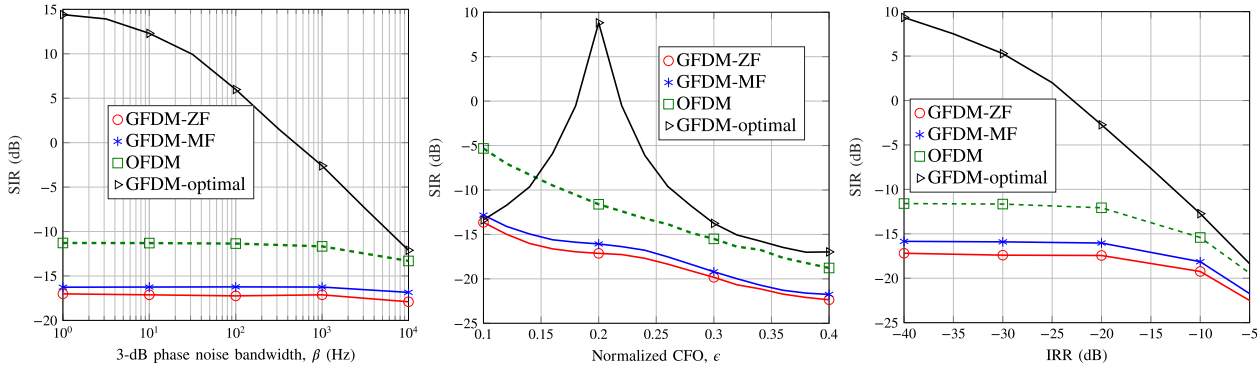

Fig. 3. Uplink SIR versus 3-dB phase noise bandwidth, normalized CFO and IRR.

and Fig. 2b for higher values of β and ϵ can be due to these exponential terms.

Fig. 2c shows that residual SI increases with increasing IQ imbalance. In this figure, $\beta = 10$ Hz and $\epsilon = 0.1$ are fixed and IRR is changed. This figure depicts the effects of IQ imbalance on the performance of the SI cancellation techniques. Clearly, all of them rapidly degrade with the increasing IQ imbalance. Finally, OFDM achieves lower residual SI than GFDM does. The reason may be that non-orthogonal subcarriers of GFDM leads to more interference.

D. Uplink and Downlink SIR

We next verify the uplink and downlink SIR expressions (37) and (44) via simulations. Moreover, we compare GFDM with the optimal SIR-maximizing receiver filter (legend GFDM-optimal) with GFDM with matched filter receiver (legend GFDM-MF) and GFDM-ZF. We derive the optimal filter for the parameter values $\beta = 50$ Hz, $\epsilon = 0.2$, and IRR $= -37.5$ dB, and use this derived filter for all other parameter values. The average transmit powers in uplink and downlink are assumed equal, i.e., $\alpha = \alpha_s$.

Fig. 3 plots the uplink SIR as a function of 3-dB phase noise bandwidth, normalized CFO and IRR. GFDM-MF, GFDM-ZF, GFDM with optimal receiver filters and OFDM are compared. Solid and dashed lines represent GFDM and OFDM, respectively. There are four or five marker points per each line. These represent the simulated points. For clarity, more simulation points are not shown.

In all of the three sub figures, theoretical uplink SIR (37) and numerical simulation result match perfectly, a verification of our derivations.

Fig. 3a illustrates SIR versus phase noise (β) for a 20% CFO and -37.5 dB IQ imbalance. Obviously, the GFDM-optimal curve degrades the most with increasing phase noise β. We also see that GFDM-optimal always achieve higher SIR than the others, e.g., for a 10 Hz phase noise, 25 dB higher SIR than full-duplex OFDM. A surprising observation is that OFDM achieves higher SIR GFDM-MF and GFDM-ZF. The reason is that GFDM uses non-orthogonal subcarriers, which generate some mutual interference, which will penalize the SIR measure. Clearly, ZF and MF strategies are not sufficient to mitigate this effect. This however can be reversed by the use of optimal receiver filters.

In Fig. 3b, the SIR is plotted as a function of CFO for a 50 Hz phase noise and -37.5 dB IQ imbalance. GFDM-ZF, GFDM-MF and OFDM reduce SIR for large CFOs. However, these methods are outperformed by the optimal-filter based GFDM, e.g., for CFO $\epsilon = 0.2$, it achieves 20 dB more SIR than OFDM. Although the optimal filter and GFDM achieves lower SIR than OFDM for small CFO, e.g. $\epsilon = 0.1$, since this fitter was optimized for $\epsilon = 0.2$. However, the receiver filter can be optimized for lower CFO to improve the SIR.

Fig. 3c represents the SIR versus IQ imbalance (measured by IRR) for fixed phase noise ($\beta = 50$ Hz) and CFO ($\epsilon = 0.2$). In all cases, increasing IQ imbalance degrades the SIR. Furthermore, GFDM-optimal outperforms OFDM, e.g., 17 dB gain is possible at -30 dB IQ imbalance.

Fig. 4 plots the downlink SIR as a function of 3-dB phase noise bandwidth, normalized CFO and IRR. GFDM-MF, GFDM-ZF, GFDM with optimal receiver filters and OFDM are compared. Solid and dashed lines represent GFDM and OFDM, respectively. There are four or five marker points per each line. These represent the simulated points. For clarity, more simulation points are not shown.

This figure shows a perfect match between theoretical (44) and simulations results. In all cases, OFDM achieves higher SIR than GFDM-MF and GFDM-ZF. Fig. 4a shows SIR versus phase noise β for CFO ($\epsilon = 0.2$) and IQ imbalance (IRR $= -37.5$ dB). Increasing phase noise (β) decreases SIR in all cases. However, the solution is to use optimal filter based GFDM, which outperforms the others and significantly increase the SIR, e.g., for $\beta = 10$ Hz, it achieves an SIR 4 dB higher than OFDM.

Fig. 4b illustrates the SIR as a function of normalized CFO for phase noise ($\beta = 50$ Hz) and IQ imbalance (IRR $= -37.5$ dB). For GFDM-MF and GFDM-ZF and OFDM, increasing CFO (ϵ) directly amounts to the decrease of SIR. However, similar to Fig. 4a, GFDM-optimal alleviates this problem and achieves higher SIR than others, e.g. for $\epsilon = 0.2$, it achieves 4 dB more than OFDM. Similar to Fig. 3, by adjusting optimized point over the range of small CFO, the SIR can be improved.

In Fig. 4c, the SIR is plotted versus IQ imbalance measured by IRR for phase noise ($\beta = 50$ Hz) and CFO ($\epsilon = 0.2$). In all

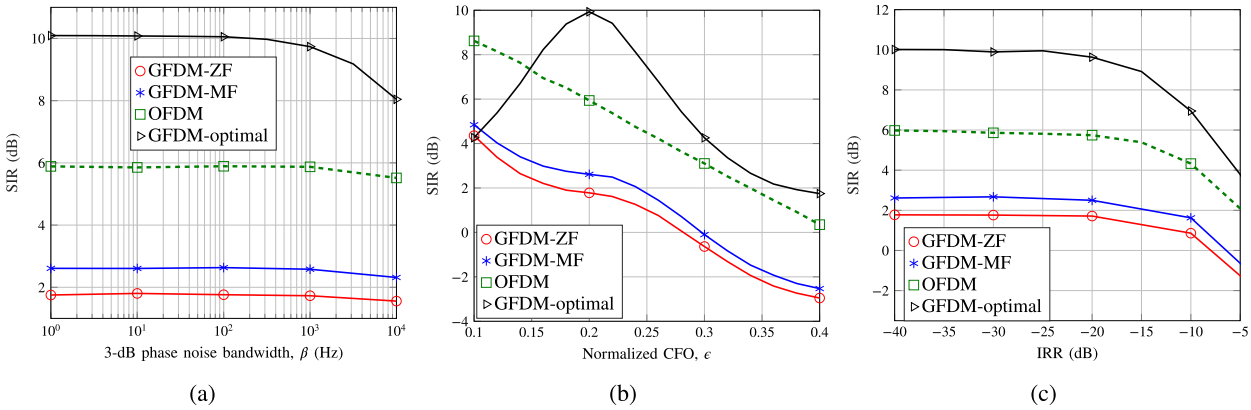

Fig. 4. Downlink SIR versus 3-dB phase noise bandwidth, normalized CFO and IRR.

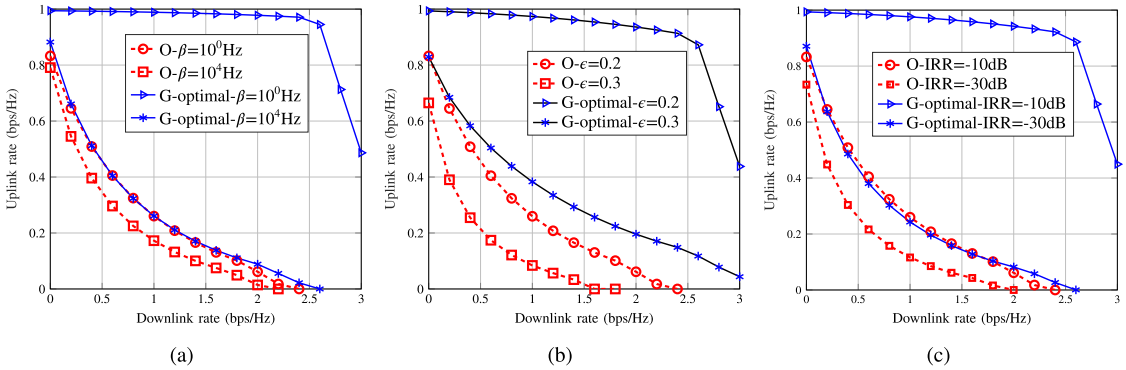

Fig. 5. Rate regions parameterized by 3-dB phase noise bandwidth, normalized CFO and IRR.

cases, more IQ imbalance (higher values of the IRR) degrades the SIR. However, this problem can be mitigated by the use of the optimal filters, which achieves higher SIR than OFDM. For example, for a -30 dB IQ imbalance, GFDM-optimal achieves 4 dB more in SIR than OFDM.

The main lesson of Figs. 3 and 4 is that RF impairments degrade the performance of GFDM-MF and GFDM-ZF much more than that of OFDM. This makes sense since GFDM relies on non-orthogonal waveforms. Fortunately, this problem can be rectified with use of the proposed GFDM optimal receiver filters in both uplink and downlink. Indeed, in uplink, the optimal filter reduces the influence of residual SI power and self-interference caused by RF impairments. Moreover, in downlink, since no SI cancellation is employed, receiver filter design can be used to suppress the uplink-user interference and achieve higher SIR.

E. Achievable Rate Region

Fig. 5 shows the rate regions parameterized by phase noise bandwidth, normalized CFO and IQ imbalance. The solid lines and dashed lines represent GFDM and OFDM. This figure includes analytical results only, no simulations. "G" and "O" stands for GFDM and OFDM. Since we found earlier that OFDM outperforms GFDM with ZF and MF filters, only GFDM with optimal uplink and downlink filters (43) and (49) is compared with OFDM.

In Fig. 5a, the rate region is evaluated for CFO ($\epsilon = 0.2$) and IQ imbalance (-37.5 dB) and for phase noise values $\beta = 10^0, 10^4$ Hz. Obviously, higher phase noise results in lower maximum uplink rate. Moreover, GFDM-Optimal achieves higher uplink rate than OFDM, e.g., for downlink rate of 1.5 bps/Hz and 1 Hz phase noise, the uplink rate increases 500% over OFDM.

In Fig. 5b, the rate region is evaluated for fixed phase noise (50 Hz) and IQ imbalance (-37.5 dB) and two values of CFO $\epsilon = 0.2, 0.3$. Clearly, increasing CFO ϵ decreases the uplink rate, but this trend can be countered by our optimal filter. For example, with $R_c = 1.5$ bps/Hz and $\epsilon = 0.2$, the optimal filter based GFDM achieves an uplink rate 300% more than OFDM. Finally, Fig. 5c considers phase noise ($\beta = 50$ Hz) and CFO ($\epsilon = 0.2$) and IRR $= -30, -10$ dB. Similar to the two other cases, the maximum uplink rate decreases with more IQ imbalance, and the optimal filters provide higher rates, e.g., $R_c = 1.5$ bps/Hz and IRR $= -30$ dB, achievable uplink rate for the optimal filter is five times greater than OFDM. All of these results indicate the benefits of the optimal receiver filter.

VII. Conclusion

This paper investigated a GFDM full-duplex transceiver in the presence of three common RF impairments – phase noise, CFO and IQ imbalance. The purpose of the investigation is to provide a comprehensive and comparative evaluation of GFDM, a potential alternative to OFDM in future communication standards.

To this end, we considered a simple network of a full-duplex base-station and half-duplex uplink and downlink users. This network helps to delineate the interplay among the various forms of interference signals and to determine their overall impact. In the uplink, we investigated both analog and digital SI cancellations and derived residual SI and desired signal powers in closed-form. For the downlink, we derived both desired signal and co-channel interference powers. For both uplink and downlink, the SIR, receiver filters for maximizing the SIR, the rates, and the closed-form optimized rate region were derived. A computational algorithm for the rate region was developed. We presented simulation results to verify the analytical derivations.

Our results cast light on the impact of the RF impairments on the performance of the SI cancellation methods. Analog linear cancellation is less sensitive to these impairments, but digital linear cancellation and complimentary digital linear cancellation can be highly sensitive. GFDM then performs worse than OFDM. The reason is that GFDM uses non-orthogonal sub-carriers, and their interaction with RF impairments ends up generating more interference. However, the good news is that GFDM has built-in degrees-of-freedom due to the transmit and receive side filters. They can be optimized to mitigate the effects of RF impairments. For example, GFDM with optimal filters readily outperforms GFDM-MF or OFDM-ZF in terms of SIR and rates. Furthermore, while OFDM outperforms GFDM in terms of rate and SIR in some scenarios, the optimal filter based GFDM sometimes provides 500% more rate than OFDM.

While this paper investigated the three most common RF impairments, this area is a fertile rich ground for many important research problems. We mention a few here. First, amplifier non-linearity strongly affects the SI cancellation methods and increases residual SI power, which could thus be investigated. Second, favorable spectral properties of GFDM can be exploited for cognitive radio networks where interference has to be managed and controlled. Thus, GFDM full-duplex radios and RF impairments could be investigated for cognitive radio networks. Third, this work was limited to a single cell system. However, practical cellular networks consist of multiple cells and are subject to both inter-cell and intra-cell interference signals. It is imperative to investigate how the multi-cell interference will affect the performance of GFDM full-duplex base-stations.

APPENDIX A
PROOF OF *PROPOSITION 1*

Let us define implicit function $F(\alpha,\alpha_s)=R^{down}(\alpha,\alpha_s)-R_c=0$ which maps α onto α_s implicitly. The derivation of $R^{up}(\alpha,\alpha_s)$ with respect to α_s can be written as

$$\frac{dR^{up}(\alpha,\alpha_s)}{d\alpha_s}=\frac{\partial R^{up}(\alpha,\alpha_s)}{\partial\alpha_s}+\frac{\partial R^{up}(\alpha,\alpha_s)}{\partial\alpha}\frac{d\alpha}{dF(\alpha,\alpha_s)}\frac{dF(\alpha,\alpha_s)}{d\alpha_s}. \quad (53)$$

From algebratic fractions in (51), it can be readily proved that $R^{up}(\alpha,\alpha_s)$ is monotonically increasing over α_s and monotonically decreasing over α, while $R^{down}(\alpha,\alpha_s)$ is monotonically increasing over α and monotonically decreasing over α_s. By exploiting these properties, we can show that $\frac{\partial R^{up}(\alpha,\alpha_s)}{\partial\alpha_s}$ and $\frac{dF(\alpha,\alpha_s)}{d\alpha}$ are positive, while $\frac{\partial R^{up}(\alpha,\alpha)}{\partial\alpha}$ and $\frac{dF(\alpha,\alpha_s)}{d\alpha_s}$ are negative. Thus, $\frac{dR^{up}(\alpha,\alpha_s)}{d\alpha_s}$ is positive and $R^{up}(\alpha,\alpha_s)$ is monotonically increasing over α_s, which transforms the objective function of optimization problem (52) $R^{up}(\alpha,\alpha_s)$ to α_s.

According to behavior of $R^{down}(\alpha,\alpha_s)$ over α and α_s, if $R^{down}(\alpha,\alpha_s)=R_c\le R_{th}=R^{down}(P_{\max},P_{\max})$, it is required to $\alpha\le P_{\max}$ or $\alpha_s\ge P_{\max}$. Thus, in this case, the solution is $\alpha_s^{opt}=P_{\max}$ and $\alpha^{opt}<P_{\max}$. Otherwise, when $R^{down}(\alpha,\alpha_s)=R_c\ge R_{th}$, α_s^{opt} is derived by considering $\alpha^{opt}=P_{\max}$. The proof of *Proposition 1* is completed.

REFERENCES

[1] Z. Zhang, K. Long, A. V. Vasilakos, and L. Hanzo, "Full-duplex wireless communications: Challenges, solutions, and future research directions," *Proc. IEEE*, vol. 104, no. 7, pp. 1369–1409, Jul. 2016.

[2] J. Jeong *et al.*, "Eigendecomposition-based GFDM for interference-free data transmission and pilot insertion for channel estimation," *IEEE Trans. Wireless Commun.*, vol. 17, no. 10, pp. 6931–6943, Oct. 2018.

[3] N. Michailow *et al.*, "Generalized frequency division multiplexing for 5th generation cellular networks," *IEEE Trans. Commun.*, vol. 62, no. 9, pp. 3045–3061, Sep. 2014.

[4] Z. Na *et al.*, "Turbo receiver channel estimation for GFDM-based cognitive radio networks," *IEEE Access*, vol. 6, pp. 9926–9935, 2018.

[5] A. Mohammadian, M. Baghani, and C. Tellambura, "Optimal power allocation of GFDM secondary links with power amplifier nonlinearity and ACI," *IEEE Wireless Commun. Lett.*, vol. 8, no. 1, pp. 93–96, Feb. 2019.

[6] Z. Wang, L. Mei, X. Sha, and V. C. M. Leung, "Minimum BER power allocation for space-time coded generalized frequency division multiplexing systems," *IEEE Wireless Commun. Lett.*, vol. 8, no. 3, pp. 717–720, Jun. 2019.

[7] F. Li, K. Zheng, L. Zhao, H. Zhao, and Y. Li, "Design and performance of a novel interference-free GFDM transceiver with dual-filter," *IEEE Trans. Veh. Technol.*, vol. 68, no. 5, pp. 4695–4706, May 2019.

[8] Z. Na, J. Lv, F. Jiang, M. Xiong, and N. Zhao, "Joint subcarrier and subsymbol allocation based simultaneous wireless information and power transfer for multiuser GFDM in IoT," *IEEE Internet Things J.*, vol. 6, no. 4, pp. 5999–6006, Aug. 2019.

[9] F. Tian *et al.*, "A novel concatenated coded modulation based on GFDM for access optical networks," *IEEE Photon. J.*, vol. 10, no. 2, Apr. 2018, Art. no. 7200808.

[10] M. Mohammadi, H. A. Suraweera, Y. Cao, I. Krikidis, and C. Tellambura, "Full-duplex radio for uplink/downlink wireless access with spatially random nodes," *IEEE Trans. Commun.*, vol. 63, no. 12, pp. 5250–5266, Dec. 2015.

[11] M. Mohammadi, H. A. Suraweera, and C. Tellambura, "Uplink/downlink rate analysis and impact of power allocation for full-duplex cloud-RANs," *IEEE Trans. Wireless Commun.*, vol. 17, no. 9, pp. 5774–5788, Sep. 2018.

[12] E. Park, J. Bae, H. Ju, and Y. Han, "Resource allocation for full-duplex systems with imperfect co-channel interference estimation," *IEEE Trans. Wireless Commun.*, vol. 18, no. 4, pp. 2388–2400, Apr. 2019.

[13] M. Zhou, H. Li, N. Zhao, S. Zhang, and F. R. Yu, "Feasibility analysis and clustering for interference alignment in full-duplex-based small cell networks," *IEEE Trans. Commun.*, vol. 67, no. 1, pp. 807–819, Jan. 2019.

[14] X. Xia, K. Xu, D. Zhang, Y. Xu, and Y. Wang, "Beam-domain full-duplex massive MIMO: Realizing co-time co-frequency uplink and downlink transmission in the cellular system," *IEEE Trans. Veh. Technol.*, vol. 66, no. 10, pp. 8845–8862, Oct. 2017.

[15] K. Xu, Z. Shen, Y. Wang, X. Xia, and D. Zhang, "Hybrid time-switching and power splitting SWIPT for full-duplex massive MIMO systems: A beam-domain approach," *IEEE Trans. Veh. Technol.*, vol. 67, no. 8, pp. 7257–7274, Aug. 2018.

[16] Y. Liu, P. Roblin, X. Quan, W. Pan, S. Shao, and Y. Tang, "A full-duplex transceiver with two-stage analog cancellations for multipath self-interference," *IEEE Trans. Microw. Theory Technol.*, vol. 65, no. 12, pp. 5263–5273, Dec. 2017.

[17] A. Sahai, G. Patel, C. Dick, and A. Sabharwal, "On the impact of phase noise on active cancelation in wireless full-duplex," *IEEE Trans. Veh. Technol.*, vol. 62, no. 9, pp. 4494–4510, Nov. 2013.

[18] C. D. Nwankwo, L. Zhang, A. Quddus, M. A. Imran, and R. Tafazolli, "A survey of self-interference management techniques for single frequency full duplex systems," *IEEE Access*, vol. 6, pp. 30242–30268, 2018.
[19] M. Duarte, "Full-duplex wireless: Design, implementation and characterization," Ph.D. Dissertation, Dept. Elect. Eng., Rice Univ., Houston, TX, USA, 2012.
[20] S. Li and R. D. Murch, "An investigation into baseband techniques for single-channel full-duplex wireless communication systems," *IEEE Trans. Wireless Commun.*, vol. 13, no. 9, pp. 4794–4806, Sep. 2014.
[21] D. Korpi, L. Anttila, V. Syrjälä, and M. Valkama, "Widely linear digital self-interference cancellation in direct-conversion full-duplex transceiver," *IEEE J. Sel. Areas Commun.*, vol. 32, no. 9, pp. 1674–1687, Sep. 2014.
[22] X. Xia, D. Zhang, K. Xu, W. Ma, and Y. Xu, "Hardware impairments aware transceiver for full-duplex massive MIMO relaying," *IEEE Trans. Signal Process.*, vol. 63, no. 24, pp. 6565–6580, Dec. 15, 2015.
[23] R. Li, A. Masmoudi, and T. Le-Ngoc, "Self-interference cancellation with nonlinearity and phase-noise suppression in full-duplex systems," *IEEE Trans. Veh. Technol.*, vol. 67, no. 3, pp. 2118–2129, Mar. 2018.
[24] V. Syrjälä, M. Valkama, L. Anttila, T. Riihonen, and D. Korpi, "Analysis of oscillator phase-noise effects on self-interference cancellation in full-duplex OFDM radio transceivers," *IEEE Trans. Wireless Commun.*, vol. 13, no. 6, pp. 2977–2990, Jun. 2014.
[25] F. Shu, J. Wang, J. Li, R. Chen, and W. Chen, "Pilot optimization, channel estimation, and optimal detection for full-duplex OFDM systems with IQ imbalances," *IEEE Trans. Veh. Technol.*, vol. 66, no. 8, pp. 6993–7009, Aug. 2017.
[26] L. Samara, M. Mokhtar, Ö. Özdemir, R. Hamila, and T. Khattab, "Residual self-interference analysis for full-duplex OFDM transceivers under phase noise and I/Q imbalance," *IEEE Commun. Lett.*, vol. 21, no. 2, pp. 314–317, Feb. 2017.
[27] W. Li, J. Lilleberg, and K. Rikkinen, "On rate region analysis of half- and full-duplex OFDM communication links," *IEEE J. Sel. Areas Commun.*, vol. 32, no. 9, pp. 1688–1698, Sep. 2014.
[28] Z. Xiao, Y. Li, L. Bai, and J. Choi, "Achievable sum rates of half- and full-duplex bidirectional OFDM communication links," *IEEE Trans. Veh. Technol.*, vol. 66, no. 2, pp. 1351–1364, Feb. 2017.
[29] X. Quan, Y. Liu, S. Shao, C. Huang, and Y. Tang, "Impacts of phase noise on digital self-interference cancellation in full-duplex communications," *IEEE Trans. Signal Process.*, vol. 65, no. 7, pp. 1881–1893, Apr. 2017.
[30] B. Lim and Y. Ko, "SIR analysis of OFDM and GFDM waveforms with timing offset, CFO, and phase noise," *IEEE Trans. Wireless Commun.*, vol. 16, no. 10, pp. 6979–6990, Oct. 2017.
[31] S. Han, Y. Sung, and Y. H. Lee, "Filter design for generalized frequency-division multiplexing," *IEEE Trans. Signal Process.*, vol. 65, no. 7, pp. 1644–1659, Apr. 2017.
[32] H. Cheng, Y. Xia, Y. Huang, L. Yang, and D. P. Mandic, "Joint channel estimation and Tx/Rx I/Q imbalance compensation for GFDM systems," *IEEE Trans. Wireless Commun.*, vol. 18, no. 2, pp. 1304–1317, Feb. 2019.
[33] B. Lim and Y. Ko, "Multiuser interference cancellation for GFDM with timing and frequency offsets," *IEEE Trans. Commun.*, vol. 67, no. 6, pp. 4337–4349, Jun. 2019.
[34] D. Gaspar, L. Mendes, and T. Pimenta, "GFDM BER under synchronization errors," *IEEE Commun. Lett.*, vol. 21, no. 8, pp. 1743–1746, Aug. 2017.
[35] W. Chung, D. Hong, R. Wichman, and T. Riihonen, "Interference cancellation architecture for full-duplex system with GFDM signaling," in *Proc. Eur. Signal Process. Conf.*, Budapest, Hungary, 2016, pp. 788–792.
[36] A. Mohammadian and C. Tellambura, "Full-duplex GFDM radio transceivers in the presence of phase noise, CFO and IQ imbalance," in *Proc. IEEE Int. Conf. Commun.*, May 2019, pp. 1–6.
[37] G. H. Golub and C. F. Van Loan, *Matrix Computations*, vol. 3. Baltimore, MD, USA: JHU Press, 2012.
[38] M. Sadek, A. Tarighat, and A. H. Sayed, "A leakage-based precoding scheme for downlink multi-user MIMO channels," *IEEE Trans. Wireless Commun.*, vol. 6, no. 5, pp. 1711–1721, May 2007.

Amirhossein Mohammadian received the B.Sc. and M.Sc. degrees in electrical engineering from the Amirkabir University of Technology, Tehran, Iran, in 2014 and 2017, respectively. He is currently working toward the Ph.D. degree in electrical engineering with the University of Alberta, Edmonton, AB, Canada. His current research interests include wireless communication, full-duplex transmission, cognitive radio networks, dirty RF and MIMO structure.

Chintha Tellambura received the B.Sc. degree in electronics and telecommunications from the University of Moratuwa, Moratuwa, Sri Lanka, the M.Sc. degree in electronics from Kings College, University of London, London, U.K., and the Ph.D. degree in electrical engineering from the University of Victoria, Victoria, BC, Canada.

He was with Monash University, Australia, from 1997 to 2002. Since 2002, he has been with the Department of Electrical and Computer Engineering, University of Alberta, where he is currently a Full Professor. He has authored or coauthored more than 560 journal and conference papers, with an h-index of 72 (Google Scholar). He has supervised or co-supervised 66 M.Sc., Ph.D., and PDF trainees. His current research interests include cognitive radio, heterogeneous cellular networks, fifth-generation wireless networks, and machine learning algorithms. He was elected as a fellow of The Canadian Academy of Engineering in 2017. He was the recipient of the best paper awards from the IEEE International Conference on Communications in 2012 and 2017. He is the winner of the prestigious McCalla Professorship and the Killam Annual Professorship from the University of Alberta. He was as an Editor for the IEEE TRANSACTIONS ON COMMUNICATIONS from 1999 to 2012 and IEEE TRANSACTIONS ON WIRELESS COMMUNICATIONS from 2001 to 2007. He was an Area Editor for *Wireless Communications Systems and Theory* from 2007 to 2012.

Mikko Valkama received the M.Sc. (Tech.) and D.Sc. (Tech.) degrees (both with honors) in electrical engineering from Tampere University of Technology, Tampere, Finland, in 2000 and 2001, respectively. He is currently Full Professor and Department Head of Electrical Engineering at newly formed Tampere University (TAU), Finland. His general research interests include radio communications, radio localization, and radio-based sensing, with particular emphasis on 5G and beyond mobile radio networks. In 2002, he was the recipient of the Best Doctoral Thesis-Award by the Finnish Academy of Science and Letters for his dissertation entitled "Advanced I/Q signal processing for wideband receivers: Models and algorithms." In 2003, he was working as a visiting Postdoctoral research fellow with the Communications Systems and Signal Processing Institute with SDSU, San Diego, CA, USA.